Tracking marine mammals in 3D using electronic tag data

Christophe Laplanche[a,b], Tiago A. Marques[c], Len Thomas[c]

[a] *Université de Toulouse; INP, UPS; EcoLab (Laboratoire Ecologie Fonctionnelle et Environnement); ENSAT, Avenue de l'Agrobiopole, 31326 Castanet Tolosan, France*
[b] *CNRS; ECOLAB; 31326 Castanet Tolosan, France*
[c] *Centre for Research into Ecological and Environmental Modelling, The Observatory, Buchanan Gardens, University of St Andrews St Andrews, KY16 9LZ, Scotland, UK*

Abstract

running title: 3D marine mammal tracking
word count (including tables, figure captions and references): 7858

1. Information about at depth behaviour of marine mammals is fundamental yet very hard to obtain from direct visual observation. Animal borne multi-sensor electronic tags provide a unique window of observation into such behaviours.
2. Electronic tag sensors allow the estimation of the animal's 3-dimensional (3D) orientation, depth, and speed. Using tag flow noise level to provide an estimate of animal speed we extend existing approaches of 3D track reconstruction by allowing the direction of movement to differ from that of the animal's longitudinal axis.
3. Data are processed by a hierarchical Bayesian model that allows processing of multi-source data, accounting for measurement errors, and testing hypotheses about animal movement by comparing models.
4. We illustrate the approach by reconstructing the 3D track of a 52-minute deep dive of a Blainville's beaked whale *Mesoplodon densirostris* adult male fit with a digital tag (DTAG) in the Bahamas. At depth, the whale alternated regular movements at large speed (> 1.5 m/s) and more complex movements at lower speed (< 1.5 m/s) with differences between movement and longitudinal axis directions of up to 28°. The reconstructed 3D track agrees closely with independent acoustic-based localizations.

5. The approach is potentially applicable to study the underwater behaviour (e.g. response to anthropogenic disturbances) of a wide variety of species of marine mammals fitted with triaxial magnetometer and accelerometer tags.

Keywords: dead reckoning, animal movement modelling, electronic tag, hierarchical Bayesian modelling, track reconstruction, triaxial magnetometer and accelerometer, flow noise

1. Introduction

The use of animal borne autonomous recording tags to collect information for inferences on movement, ecology, physiology and behaviour is becoming widespread, providing an unprecedented window into these biological processes and leading to otherwise unattainable discoveries, especially at sea where animal behaviour is hard to observe directly (Ropert-Coudert & Wilson, 2005; Bograd *et al.*, 2010).

Initially used simply to identify animals, over time tags became equipped with thermometers and barometers, followed by accelerometers, magnetometers, gyroscopes, microphones, hydrophones, GPSs, and even video (e.g. Johnson *et al.*, 2009; Burgess, 2009; Marshall *et al.*, 2007; Rutz & Troscianko, 2013). Some tags provide direct information on location while others do not. For those that do, say via GPS or radio tracking, a common approach has been to use state space models or hidden Markov models to reconstruct two dimensional tracks (e.g. Jonsen *et al.*, 2012; Beyer *et al.*, 2013; Langrock *et al.*, 2014). However, most marine mammals spend a large proportion of their time at depth, hence accounting for the depth component might be fundamental, depending on each study's objectives (e.g. Tracey *et al.*, 2014).

Published tracks in 3 dimensions (3D) are based on some form of dead reckoning (Wilson *et al.*, 2007): each position is predicted by updating the previous time step position considering an estimate of the animal's current direction and speed. One option is to infer animal 3D speed from 3D orientation (computed from accelerometer and magnetometer data) and vertical speed (from depthmeter data). However, this is sensitive to error in depth measurements, notably when animal movement is close to horizontal. This has led to estimating speed from other sources than depthmeters, namely tag flow noise (e.g. Simon *et al.*, 2009; Ware *et al.*, 2011). All such methods

have required the assumption that the direction of animal movement coincides with the direction of its longitudinal (rostro-caudal for a whale) axis, i.e. the animal moves towards where it is pointing. If this does not hold, bias can be expected, and the resulting track will be unreliable (Johnson *et al.*, 2009). Further, errors accumulate over time, a phenomena referred to as drift (Wilson *et al.*, 2007). Additional drifting due to external factors can occur (e.g. Shiomi *et al.*, 2008). Therefore, while tags are very useful to establish relative positions of animals, inferring absolute position is questionable with existing procedures: the term *pseudo-track* is used to reinforce the notion that absolute position is unknown (Hazen *et al.*, 2009). Also for this reason, dead-reckoning tracks are often "anchored" to known positions (e.g. Zimmer *et al.*, 2005; Hazen *et al.*, 2009; Friedlaender *et al.*, 2009). These are sometimes referred to as *geo-referenced* tracks, to convey the notion of absolute position on the earth sphere. However, measurement error in positions is typically ignored, and the way the pseudo-track is combined with these is not explicitly described (e.g. Davis *et al.*, 2001; Mitani *et al.*, 2003; Tyson *et al.*, 2012). Nonetheless, implementation details can have considerable impact on the estimated track, as well as (if estimated) on its precision.

We consider DTAGs (Johnson & Tyack, 2003) as an example. DTAGs include triaxial accelerometer and magnetometer sensors, a pressure sensor (sampling rate up to 50 Hz), and two hydrophones (up to 192 kHz) (Johnson & Tyack, 2003). Other tags (e.g. "OpenTag", Loggerhead Instruments, Sarasota, FL, USA) include triaxial magnetometers and accelerometers. Around 20 marine mammal species ($>$ 1000 deployments) including whales, dolphins and pinnipeds have been fitted with DTAGs (Mark Johnson, pers. comm.). Such tags have become widespread in marine mammal studies, allowing inferences about at depth behaviour and ecophysiology (e.g. Watwood *et al.*, 2006; Shaffer *et al.*, 2013). DTAGs were originally developed to infer behaviour and relative movement rather than absolute location, having been used extensively for this purpose – e.g., recent work on feeding behaviour in baleen whales (e.g. Simon *et al.*, 2012; Ware *et al.*, 2014, and references therein). However, DTAG data have been used to reconstruct 3D dives of animals (e.g. Davis *et al.*, 2001; Mitani *et al.*, 2003; Johnson & Tyack, 2003; Madsen *et al.*, 2005). Bespoke software is now available to process tag data into tracks (the R packages `animalTrack`, Farrell & Fuiman (2014), and `TrackReconstruction`, Battaile (2014), and to depict 3D tracks `Trackplot`, Ware *et al.* (2006)). An estimated position without an associated measure of uncertainty can be misleading, providing overconfidence in the reported esti-

mate. Nonetheless existing software does not provide uncertainty on position estimates, so these are never reported.

Extending dead reckoning and georeferencing methods described earlier, we develop a new way to use magnetometer and accelerometer tag data to reconstruct 3D tracks and estimate associated uncertainty. We explicitly (1) incorporate measurement error, both from the tag and from estimated positions, in the input data and propagate this error through to the estimated track; (2) include information about animal speed both from change in depth given orientation and from tag flow noise; and (3) utilize the additional information from both sources of speed information to relax the assumption that the animal moves in the direction it is pointed. Our model is superficially similar to well-known 2D random walk models by, e.g., Jonsen *et al.* (2005), Morales *et al.* (2004) and McClintock *et al.* (2012) in that, like them, we model animal speed (i.e. step length) and movement direction in discrete time and continuous space, and use Bayesian methods to link models to data. However, assumptions about animal movement differ. Random walk models make distributional assumptions about step length and direction (or turning angle), hence resulting track estimates are a combination of the assumed movement model and the input data (filtered through the observation process); by contrast we do not make such assumptions, hence our estimated tracks are a function of the data and observation process alone. In this sense, our approach is more "data focused", but is also more reliant on having high frequency, high quality data to produce a realistic track. We return to these issues in the Discussion.

We illustrate our method by reconstructing a 52-minute dive of a tagged Blainville's beaked whale *Mesoplodon densirostris* (Laplanche *et al.*, 2015), for which independent underwater localizations are available. These are not used in model fitting; instead we use them to evaluate the accuracy of the estimated track derived from tag data alone. Finally, we discuss the capabilities of the approach and possible improvements.

2. Materials and methods

2.1. Tag measurements and coordinate systems

We consider three coordinate systems (or frames) to accurately describe animal movement and tag data: (1) the Earth frame, a cartographic projected coordinate system (x-axis south-north, positive north; y-axis east-west, positive west; z-axis bottom-up, positive up; origin is some arbitrary

location at the sea surface), (2) the animal frame (x-axis, longitudinal axis, positive forward; y-axis, right-left axis, positive left; z-axis, dorso-ventral axis, positive up; origin is the geometric center of the animal), and (3) the tag frame (x-, y-, z-axes are internally defined; origin is the center of the tag) – this latter frame is required because the tag is not always placed with the same orientation on the animal.

An animal's 3D track is the time-series of its 3D location; more specifically the 3D Cartesian coordinates of the origin of the animal frame in the Earth frame, denoted $\boldsymbol{x}(t) = (x(t), y(t), z(t))$ at time t. Animal 3D speed is the time derivative of $\boldsymbol{x}(t)$; the speed of translation of the animal frame in the Earth frame, denoted $\boldsymbol{v}(t) = (v_x(t), v_y(t), v_z(t))$. The orientation of a 3D object in space is unambiguously described in terms of heading h (rotation to the z-axis, $h \in (-180°, 180°]$), pitch p (y-axis, $p \in (-90°, 90°]$), and roll r (x-axis, $r \in (-180°, 180°]$) with respect to some frame of reference. The animal's 3D orientation at time t is represented by its heading $h(t)$ (positive Eastwards), pitch $p(t)$ (positive upwards) and roll $r(t)$ (positive rightwards), with respect to the Earth frame.

Tag data are not directly available in the Earth frame. Accelerometer and magnetometer measure the Earth's gravitationnal and magnetic fields in the tag frame. The conversion of Earth's gravitationnal and magnetic fields between animal and Earth frames is achieved *via* rotation matrices described in the next section. The conversion of raw accelerometer and magnetometer data in the tag frame into the animal frame is achieved in a similar way. Description of the latter process, together with the processing of acoustic data into flow noise level, is deferred to Section 2.5.

2.2. The statistical model

We describe the full statistical model here. Approximations used in practice for computational efficiency are described in Section 2.3.

The objective is to use available tag data (Earth's gravitationnal and magnetic fields in the animal frame, depth, flow noise level), and independent positional data, if available, to infer unknown, latent variables characterizing animal movement ($\boldsymbol{x}(t)$, $\boldsymbol{v}(t)$, $h(t)$, $p(t)$, and $r(t)$). Our implementation utilizes a hierarchical Bayesian model (HBM). The overall model structure is illustrated in Figure 1, relating latent and measured variables as detailed below. For clarity the model is presented in four sections: (1) estimation of animal orientation from accelerometer, magnetometer and depth-meter measurements; (2) estimation of speed from flow noise measurement and

direction of movement from a combination of speed, orientation and change in depth; (3) track estimation, and (4) incorporation of independent positional information.

We define t_0 and t_{end} as the track start and end times, $t \in [t_0, t_{end}]$.

2.2.1. Animal 3D orientation

The expected values $\boldsymbol{A^a}(t)$ and $\boldsymbol{M^a}(t)$ of the 3D Earth gravitationnal and magnetic fields in the animal frame (superscript a) at time t are

$$\begin{aligned} \boldsymbol{A^a}(t) &= T(t)\boldsymbol{A^e} \\ \boldsymbol{M^a}(t) &= T(t)\boldsymbol{M^e}, \end{aligned} \tag{1}$$

where $T(t)$ is a rotation matrix that switches from the Earth frame to the animal frame given by

$$\begin{aligned} T(t) &= \begin{pmatrix} 1 & 0 & 0 \\ 0 & \cos r(t) & \sin r(t) \\ 0 & -\sin r(t) & \cos r(t) \end{pmatrix} \\ &\times \begin{pmatrix} \cos p(t) & 0 & \sin p(t) \\ 0 & 1 & 0 \\ -\sin p(t) & 0 & \cos p(t) \end{pmatrix} \\ &\times \begin{pmatrix} \cos h(t) & \sin h(t) & 0 \\ -\sin h(t) & \cos h(t) & 0 \\ 0 & 0 & 1 \end{pmatrix}, \end{aligned} \tag{2}$$

and $\boldsymbol{A^e}$ and $\boldsymbol{M^e}$ are the values of the 3D Earth gravitational and magnetic fields in the Earth frame (superscript e) at the tagging location and time. Given the relative small scale of most studies, ours included, compared to these 3D Earth fields, these can safely be treated as constants. They can be either measured or derived from models of the gravitational and Earth magnetic fields.

Measured (superscript *obs*) values of the Earth gravitational ($\boldsymbol{A^{a,obs}}(t)=$ and magnetic fields ($\boldsymbol{M^{a,obs}}(t)$) in the animal frame at time t are modelled as multivariate Gaussian distributions (MVN)

$$\begin{aligned} \boldsymbol{A^{a,obs}}(t) &\sim \text{MVN}(\boldsymbol{A^a}(t), \boldsymbol{\Sigma_A}(t)) \\ \boldsymbol{M^{a,obs}}(t) &\sim \text{MVN}(\boldsymbol{M^a}(t), \boldsymbol{\Sigma_M}(t)) \end{aligned} \tag{3}$$

where $\boldsymbol{\Sigma_A}(t)$ and $\boldsymbol{\Sigma_M}(t)$ are time-dependent covariance matrices (see Appendix S1 for details). The observed animal depth is

$$z^{obs}(t) \sim \text{Normal}(z(t), \sigma_z^2), z^{obs}(t) \leq 0, \tag{4}$$

where $z(t)$ is the unobserved true depth of the animal in the Earth frame and σ_z^2 is the depth-meter measurement error variance.

2.2.2. Animal speed and direction of movement

We explicitly relax what we refer in the following as the *equal pitch assumption*: that the direction of animal movement coincides with the direction of its longitudinal axis. Animal speed animal at time t is

$$\begin{cases} v_x(t) = \cos h'(t) \cos p'(t) v(t) \\ v_y(t) = -\sin h'(t) \cos p'(t) v(t) \\ v_z(t) = \sin p'(t) v(t), \end{cases} \tag{5}$$

where $v(t) = ||\boldsymbol{v}(t)||$, $h'(t)$, and $p'(t)$ are the Euclidean norm, the heading (positive Eastwards), and the pitch (positive upwards) in the Earth frame of the speed vector of the animal at time t. Differences of orientations of the longitudinal axis and the speed vector are modeled as differences in respective pitch angles

$$p'(t) \sim \text{Normal}(p(t), \sigma_p^2), \quad p'(t) \in (-90, 90], \tag{6}$$

where σ_p^2 is the variance of the pitch difference $\Delta p(t) = p(t) - p'(t)$. We refer in the following to this as the *unequal pitch assumption* and to $\Delta p(t)$ as *pitch anomaly*. A positive pitch anomaly occurs when the animal points its longitudinal axis higher than expected by its swimming direction, and vice versa (Figure 2). Pitch anomaly can be the result of a pitch and/or a heading movement in the animal frame depending on the roll. For reasons discussed later, we do not consider heading anomaly, hence assuming $h(t) = h'(t)$.

Animal speed is related to background noise level $\text{NL}(t)$ at time t assuming

$$v(t) \sim \text{Normal}(a_v + b_v \log(\text{NL}(t)), \sigma_v^2), v(t) \geq 0, \tag{7}$$

where a_v and b_v are regression parameters and σ_v is the residual standard error (Appendix S2).

2.2.3. Animal 3D track

Animal Cartesian coordinates at time $t + \Delta t$ are computed from coordinates at time t and speed:

$$\begin{cases} x(t + \Delta t) = x(t) + v_x(t) \Delta t \\ y(t + \Delta t) = y(t) + v_y(t) \Delta t \\ z(t + \Delta t) = z(t) + v_z(t) \Delta t \end{cases} \tag{8}$$

2.2.4. Independent positional information

In our application we only use information about the dive starting position, assumed to have been observed with known error. We model this as

$$\begin{cases} x^{obs}(t_0) \sim \text{Normal}(x(t_0), \sigma_x^2(t_0)) \\ y^{obs}(t_0) \sim \text{Normal}(y(t_0), \sigma_y^2(t_0)) \end{cases} \tag{9}$$

where $\sigma_x^2(t_0)$ and $\sigma_y^2(t_0)$ are known variance terms. If the absolute start position is unknown, arbitrary values are provided for $(x^{obs}(t_0), y^{obs}(t_0))$ with null variances ($\sigma_x^2(t_0) = \sigma_y^2(t_0) = 0$); estimated locations become relative to this position.

Similarly, additional animal positions might be used to improve the track reconstruction process. When at the surface these could come from visual observations, animal-borne GPS or satellite receivers. When underwater, these could come from passive (or active) acoustic localizations.

2.2.5. Priors

Prior distributions are required on all top-level random variables in the hierarchical model. Observation variance parameters are assumed known, hence not requiring priors. We also assume the relationship between measured noise level and speed is known with certainty (see Section 2.3 and Discussion). These variables are shown as grey boxes in Figure 1. The remaining top-level variables are pitch, heading and roll at each time step, for which uniform distributions are assumed:

$$\begin{cases} p(t) \sim \text{Uniform}(-90, 90) \\ h(t) \sim \text{Uniform}(-180, 180) \\ r(t) \sim \text{Uniform}(-180, 180) \end{cases} \tag{10}$$

2.3. Bayesian computation and approximating model

The model described by equations (1)-(10) is not analytically tractable; however, samples from the posterior distribution of latent variables can be simulated via Markov chain Monte Carlo (MCMC). For this, we used OpenBUGS version 3.2.1, open-source version of WinBUGS (Ntzoufras, 2009). BUGS code is available as Appendix S3. Tag data preprocessing and output postprocessing were implemented in R (R Core Team, 2013).

Initial runs showed that the full model was highly computer-intensive. Two procedures were implemented to reduce computing time, both of which mean we fit an approximation to the full model. Firstly, the model was

divided into three stages (and each stage was analyzed in turn): (i) compute animal 3D orientation (equations 1 - 4, 10); (ii) calibrate the speed-noise relationship (equation 7); (iii) compute animal 3D track (equations 5, 6, 8, 9). Uncertainty was propagated across stages by modelling stage outputs as Gaussians, with mean and variance equal to the corresponding posterior values, using this distribution as input to the next stage. However, in moving from stage (ii) to (iii) the parameters of the speed-noise model were assumed known. Secondly, in computing stages (i) and (iii), the track was divided into 1-minute pieces. Each piece was run in parallel using a high performance computing resource (HPR). Pieces were then joined and uncertainty from the end of each piece propagated to the beginning of the next (see Appendix S4 for details and discussion for possible impacts).

MCMC convergence was assessed by computing the inter-chain variances of the simulated latent variable samples across 4 chains. For each chain, once convergence was reached, $10,000$ samples were simulated; these were thinned to $1,000$ independent samples per chain, with thinning guided by analyzing the autocorrelation function of the posterior samples. Reported point estimates are posterior means, standard errors are posterior standard deviations (reported as mean $\pm$ standard error), and reported interval estimates are 2.5 % and 97.5 % posterior marginal quantile estimates.

2.4. Alternative models for pitch anomaly

The model assumes a fixed pitch anomaly standard deviation σ_p (see Discussion for a relaxation of this assumption). To investigate how pitch anomaly varied along the track we repeated the above analysis considering three different values for σ_p: 0°, 5° and 10°. These represent three different models and we denote them $\mathcal{M}_0$, $\mathcal{M}_5$ and $\mathcal{M}_{10}$, respectively.

Models were compared, for each track piece, using the Deviance Information Criterion (DIC Spiegelhalter *et al.*, 2002), a goodness-of-fit index penalized for model complexity, similar in spirit to Akaike's Information Criterion; smaller values are considered better (see Section 4 for a discussion of alternative model selection measures). Following Gelman *et al.* (2003) we estimated model complexity as $p_v = \text{var}\{-2\log[p(\theta|y)]\}/2$. The models do not share the same complexity: $\mathcal{M}_0$ is the least complex ($p'(t)$ is perfectly known given $p(t)$), which is less complex than $\mathcal{M}_5$ ($p'(t)$ estimated under the more relaxed constraint of equation (6) with $\sigma_p = 5^\circ$) which is itself less complex than $\mathcal{M}_{10}$ (even more relaxed constraint with $\sigma_p = 10^\circ$). In the Results, we report which model was favoured in each minute of the track.

2.5. Example dataset

For illustration we used a *Mesoplodon densirostris* Blainville's beaked whale adult male tagged on the 5^{th} September 2007 (tag on position: 24.3839 N, 77.5615 W) at AUTEC (Atlantic Undersea Test and Evaluation Center, an instrumented US Navy testing range in the Bahamas). AUTEC details and a different analysis of this DTAG data can be found in Ward *et al.* (2011). We illustrate the methods using the first deep dive, which lasted $51'20''$ (full tag deployment: 16 hours, 5 deep dives). *Mesoplodon densirostris* depth profiles have been modelled using behaviour states (Langrock *et al.*, 2013), and deep dives can be divided in descent, foraging and ascent phases: here the whale fluked up and initiated its dive at arbitrarily fixed $t_0 = 0$, ended its descent and started active searching for prey at $t_B = 7'50''$, stopped active searching for prey and initiated its ascent at $t_C = 35'30''$, and reached the surface at $t_{end} = 51'20''$.

The magnetic field was computed by using the IGRF11 (11^{th} Generation International Geomagnetic Reference Field) Earth's main magnetic field model (International Association of Geomagnetism and Aeronomy, Working Group V-MOD, 2010). The magnetic field at the tagging location and time was $\boldsymbol{M^e} = (25736, 3205, -35522)$ nT (declination: 7.15° W; inclination: 54.08° down). The gravitational field was $\boldsymbol{A^e} = (0, 0, -9.79)$ m/s^2. Arbitrary null values were provided for the location of the whale at the beginning of the dive ($x^{obs}(t_0) = y^{obs}(t_0) = 0$ m with $\sigma_x^2(t_0) = \sigma_y^2(t_0) = 0$ m).

Raw tag-frame accelerometer and magnetometer data were converted into animal-frame accelerometer and magnetometer data as described by Johnson & Tyack (2003). Accelerometer, magnetometer, and depth-meter data were lowpass filtered by using a 1-second, squared-window rolling mean before being downsampled at 1 Hz ($\Delta t = 1$ s). Background noise level was evaluated as the median of the absolute value of the acoustic samples over a 1-second window before being downsampled at 1 Hz. This simple procedure is robust to the presence of transient signals, in our case echolocation signals emitted by the tagged animal.

Eight independent acoustic localizations with low measurement error were available (at 7'40, 10'40, 10'44, 29'21, 29'22, 29'23, 29'24, and 29'33), obtained by cross referencing data from AUTEC range hydrophones with the known times of emission of clicks from the tag (see Ward *et al.* (2011) for details). These were ignored in the modelling, providing instead an independent comparison to our location results. For comparison, a conventional dead reckoning track was obtained based on a state space model formulation

with 4 states (x, y, z, speed) and 1 observation (depth). Heading and pitch were treated as known covariates, fitted via a Kalman filter, implemented in R.

3. Results

The dive track reconstruction (for all 3 models) on a single MCMC chain would have required 65 h of computation time on a single core of a Intel® Xeon E5-2680v2 2.8Ghz 10-core processor. This was reduced to 75 minutes using HPR (Appendix S4).

Estimates of whale heading, pitch, and roll for the complete dive are provided as Appendix S5. The standard deviations of the whale heading, pitch, and roll estimates were 0.78° (average for the whole dive, 95 % in $(0.35°, 1.31°)$), 0.35° $(0.18°, 0.54°)$, and 0.47° $(0.14°, 1.01°)$, respectively. These quantify observation measurement error in heading, pitch, and roll. Animal speed is linearly predicted from log-transformed flow noise level ($R^2 = 0.77$, Appendix S2).

DIC values are shown in Figure 3. Model $\mathcal{M}_0$ was favoured from $1'$ to $5'$. Model $\mathcal{M}_5$ performed better for the rest of the dive except for 4 dive portions (at $12'$, $18'$, $25'$, $45'$) where $\mathcal{M}_{10}$ was favoured. $\mathcal{M}_0$ better performance at the beginning of the dive (similar fit with lower complexity) can be explained by the whale's negligible pitch anomaly at this stage leading to the equal pitch assumption. The improvement provided by $\mathcal{M}_5$ and $\mathcal{M}_{10}$ for the rest of the dive (better fit despite higher complexity) suggests a non negligible pitch anomaly and consequent need for equation (6). Model $\mathcal{M}_5$ performed better than $\mathcal{M}_{10}$ for most of the dive (similar goodness-of-fit with lower complexity) indicating that the flexibility introduced by setting $\sigma_p = 5°$ should be preferred to $\sigma_p = 10°$. Nonetheless, $\mathcal{M}_{10}$ outperformed $\mathcal{M}_5$ for some dive portions (better fit despite higher complexity) with higher amplitude pitch anomaly. Overall, results strongly favor the unequal pitch assumption and $\sigma_p = 5°$. The following results are exclusively based on model $\mathcal{M}_5$, but this choice is not critical, as localization results are similar by using $\sigma_p = 10°$ (distance between tracks: 17.4 ± 14.5 m). The whale's estimated 3D track is illustrated in Figure 4 (interval estimates are provided as Appendix S5). The absolute distance between the results from the independent acoustic survey localizations and the estimated track from $\mathcal{M}_5$ is 38.3 ± 18.7 m. For comparison a standard dead-reckoning track fitted using a Kalman Filter is also shown (distance between tracks: 151.6 ± 88.9 m). Estimated speed and

pitch anomaly is illustrated in Figure 5. The whale initiated its dive with a strongly negative pitch anomaly ($-20°$), pitch anomaly rapidly reached zero ($t \in [0'00, 0'40]$) and stabilized (peak-to-peak lesser than $4°$, $t \in [2'00, 6'00]$ and up to $15°$ for $t \in [6'00, 7'50]$). At depth ($t \in [7'50, 35'30]$), the whale alternated sections with either moderate pitch anomaly variations (peak-to-peak lesser than $10°$) or strong variations (peak-to-peak up to $40°$). During the ascent ($t \in [35'30, 51'20]$), the whale had a positive pitch anomaly (between $5°$ and up to $28°$). At depth, sections of large speed were associated with moderate pitch anomaly variations and sections of low speed were associated with strong pitch anomaly variations, suggesting that the whale alternated complex rotational movements at low speed and more regular movements at higher speed. During the ascent, the whale always kept a positive pitch while the vertical speed could be negative (as low as -0.40 m/s) as illustrated in Figure S2-2 (Appendix S2). The whale alternated active fluking (strong variations in speed) and passive gliding (no variation) with a strong positive pitch anomaly for the whole ascent.

4. Discussion

We used a relatively simple "data driven" model, where expected orientation is a function of accelerometer and magnetometer measurements, expected speed is a function of measured noise and pitch anomaly is a function of speed and measured changed in depth. Measurement error on the observed quantities was assumed Gaussian, with known variance (except for variance in the speed vs. flow noise relationship, which was estimated). This approach can be expected to produce a realistic track where high quality (i.e., low error), high frequency data are available that relate closely to animal orientation and speed. DTAGs generate exactly such data. By contrast, where the data give less accurate information about animal movement or position, and/or are collected much less frequently, then it becomes necessary to include assumptions about the underlying movement behaviour of the animal in the model – for example using a biased correlated random walk, with model parameters representing centres of attraction or repulsion and correlation between time steps (e.g. McClintock *et al.*, 2012). A good example of such data is Argos satellite tags (see, e.g. McClintock *et al.*, 2015). One advantage of our approach is that the track is not constrained by assumptions about movement behaviour. Disadvantages include it: (1) requires high quality data; (2) does not incorporate biological knowledge of animal movement

behaviour (except in the specification of different error variances in different diving phases); (3) does not directly allow biological inferences about movement (in contrast with, e.g., the multi-state models of McClintock *et al.* (2012) – although such inferences could be made in a second analysis stage; (4) cannot be used for simulating tracks, since it relies on input data at each time step. Therefore, the most appropriate approach depends on the data available and the goals of the analysis.

Reconstructing 3D tracks from accelerometer, magnetometer, and depthmeter data alone, by implicitly assuming that the animal is moving in the direction of its longitudinal axis, might lead to biased inferences (see Figure 4). As illustrated in Figure S2-2 (Appendix S2), the whale's movement direction does not necessarily coincide with its longitudinal axis during the ascent. Therefore the animal is capable of having a movement direction different to its own axis, issuing a serious warning against the equal pitch assumption. The inability to estimate speed when the animal is approximately horizontal (Appendix S2) represents an additional argument against reconstructing 3D tracks from accelerometer, magnetometer, and depthmeter data alone.

Following previous work (e.g. Simon *et al.*, 2009; Ware *et al.*, 2011) we estimated speed from an independent source, modeling the speed/noise relationship using the animal's steep descent phase, formalized via a loglinear relationship. The estimated track consistency with independent acoustic locations suggests that this procedure is sensible, at least for the first 30 minutes of the dive when acoustic data were available. However, using flow noise as a proxy for animal speed has its own limitations. It can be sensitive to changes in background noise during the dive (e.g. presence of sonar, boat motor, animal sounds). Difficulties are expected if the goal is to reconstruct tracks at the surface, when other sources might contribute significantly to acoustic noise (e.g. wave lapping) – a solution for this is discussed later. Further, animal speed estimates from flow noise assume that the speed-flow noise relationship is independent of the animal orientation (discussed in more detail later).

The key advantage of including an independent estimate of speed was the ability to relax the equal pitch assumption, clearly supported by the data (Figure S2-2) and by our localization results. For example, the whale was able to be oriented upwards while moving downwards (e.g. during the ascent), with differences up to 28° between 3D orientation of its longitudinal axis and its speed vector. Consequently, accounting for complex animal movements by dissociating animal translation and rotation movements seems

necessary to produce reliable 3D tracks. We have considered a fixed, known variance for pitch anomaly and concluded that a 5° was a sensible choice for our example. Another approach might be to consider an unknown variance for pitch anomaly. Hence, provided a reasonable vague prior, variance would be estimated while reconstructing the track, and (at least in theory) a time-dependent variance might be considered.

We considered DIC as a model selection metric because it was readily implemented in OpenBUGS. We acknowledge DIC's use is controversial, and that other approaches have been suggested (see, e.g., discussion papers following Spiegelhalter *et al.* (2002, 2014)). It may, for example, be possible to implement a Gibbs Variable Selection or related approach (see O'Hara & Sillanpää (2009) for review) to estimate the posterior model probability for a model with 0 variance in pitch anomaly vs a model with a non-zero variance prior.

Pitch anomaly does not necessarily describe a pitch movement of the animal in its own frame; instead it is the difference between the animal's longitudinal axis pitch and the pitch of its speed vector (both on the Earth frame). Depending on the animal's roll, pitch anomaly can be the result of a pitch movement (in the animal frame) if roll is null or equal to $\pm 180°$, of a heading movement (in the animal frame) if roll is equal to $\pm 90°$, or a combination of both. Average roll was 4.9° (95 % in $(-39.6°, 20.5°)$) during the descent, $-5.0°$ $(-53.7°, 35.2°)$ at depth, and 1.0° $(-15.8°, 23.0°)$ during the ascent. Consequently, variations in pitch anomaly here mainly depict pitch movements (in the animal frame) slightly combined with heading movements. We have not included heading anomaly in the model. Similarly as for pitch, heading anomaly could be defined as the difference between the heading of the longitudinal axis of the animal and the heading of its speed vector. A positive heading anomaly would represent movements when the animal points its longitudinal axis more on the starboard side than expected by its swimming direction, and vice versa. The reason for not including heading anomaly in the model is that it is not possible, given the available data, to compute both pitch and heading anomalies. Considering only pitch anomaly is a parsimonious choice: the most likely explanation for the discrepancy between measured depth and the depth predicted by the 3D orientation of the animal and its speed norm is through a vertical shift of the speed vector, i.e. pitch anomaly.

The model handles four sources of errors: observation measurement errors on accelerometer/magnetometer data (Σ_A and Σ_M), on depth data (σ_z^2), and

internal errors due to differences between 3D orientations of the animal body and speed (σ_p^2), and on the prediction of speed from flow noise (σ_v^2). The model propagates measurement and process errors into parameter estimate errors. However, it still apparently underestimates the location estimates precision, as indicated by the independent acoustic localizations (Figure 4 and Appendix S5). Variances of parameter estimates are conditional on the model being true. This is strictly unrealistic, as the model still represents an oversimplification of the mechanism underlying animal 3D displacement and flow noise. Therefore, while ignoring them should be avoided, confidence intervals associated with locations should be handled with caution.

There are (at least) 4 additional sources of errors ignored by the model: (1) Strictly, the speed considered is the speed of the animal with respect to the water mass. We consequently reconstructed the track in the water mass frame, not in the Earth frame. If water speed (in the Earth frame) is not negligible with respect to animal speed (in the water mass frame), track reconstruction might be biased. Were current speeds available one could incorporate them by adding a correction term in equation (8); (2) the calibration of the orientation of the tag to the whale frame was assumed to be an error free process, and potential tag shift over time ignored. An option would be to estimate calibration angles while reconstructing the track to propagate calibration errors to uncertainties on animal 3D orientation. Further research on the impacts of this calibration procedure on DTAG based by-products is welcome; (3) while errors on the prediction of the speed from the noise level are considered (equation (7)), errors on the parameters of the relationship (a_v, b_v, σ_v) or on the relationship itself are ignored – the use of a more advanced relationship, calibrated while reconstructing the track is an interesting perspective; (4) a known error-free variance σ_p^2 was used. As mentioned earlier, an option would be to estimate σ_p^2. The consequences of assuming a known calibrated speed-noise relationship and a known variance σ_p^2 on the track reconstruction process are explored in Appendix S6.

No explicit track smoothing was implemented. The reconstructed track regularity (Figure 4) is the consequence of the estimated speed regularity (Figure 5), itself the consequence of flow noise regularity, caused by smooth animal movement. Another option to smooth the track would be to consider explicitly autocorrelation in animal 3D orientation and speed. This might help when speed could not be inferred from flow noise (e.g. tags without acoustic sensors). One possible implementation is to add two sets of latent variables, angular speeds ($v_h(t)$, $v_p(t)$, $v_r(t)$, e.g. $v_h(t) =$

$(h(t+\Delta t) - h(t))/\Delta t)$ and accelerations ($a_x(t)$, $a_y(t)$, $a_z(t)$, e.g. $a_x(t) = (v_x(t+\Delta t) - v_x(t))/\Delta t)$, assumed unbiased with known behavioral state dependent variances, . As an illustration, the angular speed statistics (mean $\pm$ standard deviation) of our whale differ across behavioral states: descent (pitch: $-1.0 \pm 3.7°/s$; heading: $0.0 \pm 2.0°/s$; roll: $0.5 \pm 3.0°/s$), at depth ($-0.8 \pm 5.5°/s$; $-0.1 \pm 5.0°/s$; $0.0 \pm 5.0°/s$), and ascent ($-0.2 \pm 3.0°/s$; $0.0 \pm 2.5°/s$; $0.0 \pm 2.2°/s$). Acceleration (3 coordinates altogether) also differ across states: descent (0.000 ± 0.091 m/s^2), at depth (0.001 ± 0.200 m/s^2), and ascent (0.000 ± 0.081 m/s^2). The latter values could also be used to smooth animal tracks computed from acoustic surveys, as described by Laplanche (2012).

One of the advantages of implementing the model in a Bayesian framework is that incorporation of additional data sources and propagating corresponding observation errors is conceptually straightforward. Acoustic based localization could be used as direct observations or provide time of arrival differences (TDOA) data instead of computed localization, by combining our model with that of Laplanche (2012), which would deal with propagating TDOA errors to localization estimates.

We made some approximations to speed up model fitting computations: (1) we broke the full model into three parts (3D orientation, speed-flow noise and track reconstruction) and (2) analyzed some parts in one minute chunks, using Gaussian distributions to cascade uncertainty between chunks (see Section 2.3 and Appendix S4). These approximations are expected to have a negligible influence on the estimated track since they concern only the variance of orientation and position. Nevertheless, we see four main drawbacks in our implementation: (1) it is not compatible with additional independent positional information (GPS or acoustic based), except for at the first time point; (2) it removes the possibility to correct for animal acceleration while computing animal orientation from accelerometer data. Although animal acceleration is negligible for large species, like the beaked whale considered here, it would be questionable for smaller, rapid species like dolphins or pinnipeds; (3) it prevents calibrating tag orientation while reconstructing the track, and (4) it removes the possibility to account for animal orientation and speed to predict flow noise and compare to data for the whole dive.

Clearly HPR are a valuable tool, giving the potential to speed up extensive computations. Whether this potential is realized is case specific: in our case, because of the independence of some latent variables over time, parts of the computation could be carried out in parallel with almost no loss in

inference accuracy. This might no longer be the case if the model were extended. Another option to reduce computation time might be implementing the model in a likelihood based approach, e.g. via an extended Kalman-filter, another research avenue we are pursuing.

Reconstructing tracks from accelerometer, magnetometer and depthmeter tag data happens routinely regardless of potential hidden dangers in doing so. The need for methods incorporating observation error and providing precision measures on estimated tracks is clear. We have shown that the approach described here, allowing (1) the estimation of speed from flow noise and consequently (2) the dissociation of the 3D orientation of the animal longitudinal axis and the 3D orientation of its speed vector, is an important step towards such goal. We suggest that practitioners should evaluate the validity of the equal pitch assumption on their species before reconstructing 3D tracks. Our methods – considering equal/unequal pitch assumption, comparing outputs and fits, and using independent localization – are an option. It allowed us to design a new descriptor on marine mammal movement: pitch anomaly. We believe that making assumptions explicit via a mathematical model is a relevant approach in gathering current knowledge about animal behavior, identifying gaps, and allowing new insights.

Acknowledgements

Access to the HPC resources of CALMIP was granted under the allocation 2014-P1421. TAM was funded under grant number N000141010382 from the Office of Naval Research (LATTE project). A number of extremely useful discussions with Mark Johnson provided insights on various aspects of this analysis. Points of view that are expressed in the present work are not to be taken to reflect the views of MJ. Jessica Ward provided comments on earlier versions of the manuscript, helped gathering the beaked whale data and provided AUTEC's independent acoustic localizations. Stacy DeRuiter provided comments and encouragement throughout. Tag data was facilitated by Peter L. Tyack. Tagging performed under US National Marine Fisheries Service research permit numbers 981-1578-02 and 981-1707-00 to PLT and with the approval of the Woods Hole Oceanographic Institution Animal Care and Use Committee. We acknowledge the considerable improvements to the paper thanks to suggestions from the reviewing process.

Data Accessibility

The DTAG data used to illustrate the methods is available from the Dryad Digital Repository: http://dx.doi.org/10.5061/dryad.138cg

Supporting information

- **Appendix S1**. Statistical model for accelerometer and magnetometer measurement errors.
- **Appendix S2**. Statistical model for speed from background noise level.
- **Appendix S3**. BUGS code.
- **Appendix S4**. Procedure to distribute track computations on a High Performance Resource (HPR).
- **Appendix S5**. Point and interval estimates of the heading, pitch, roll, and coordinates of the whale for the complete dive.
- **Appendix S6**. Investigating sensitivity to variance in pitch anomaly and flow noise relationship.

References

Battaile, B. (2014) *TrackReconstruction R package Vignette*.

Beyer, H.L., Morales, J.M., Murray, D. & Fortin, M.J. (2013) The effectiveness of Bayesian state-space models for estimating behavioural states from movement paths. *Methods in Ecology and Evolution*, **4**, 433–441.

Bograd, S.J., Block, B.A., Costa, D.P. & Godley, B.J. (2010) Biologging technologies: new tools for conservation. Introduction. *Endangered Species Research*, **10**, 1–7.

Burgess, W.C. (2009) The Acousonde: A miniature autonomous wideband recorder. *The Journal of the Acoustical Society of America*, **125**, 2588–2588.

Davis, R.W., Fuiman, L.A., Williams, T.M. & Boeuf, B.J.L. (2001) Three-dimensional movements and swimming activity of a northern elephant sea. *Comparative Biochemistry and Physiology Part A*, **129**, 759–770.

Farrell, E. & Fuiman, L. (2014) *Package "animalTrack": Animal track reconstruction for high frequency 2-dimensional (2D) or 3-dimensional (3D) movement data.*

Friedlaender, A.S., Hazen, E.L., Nowacek, D.P., N, H.P., Ware, C., Weinrich, M.T., Hurst, T. & Wiley, D. (2009) Diel changes in humpback whale *Megaptera novaeangliae* feeding behavior in response to sand lance *Ammodytes* spp. behavior and distribution. *Marine Ecology Progress Series*, **395**, 91–100.

Gelman, A., Carlin, J.B., Stern, H.S. & Rubin, D.B. (2003) *Bayesian Data Analysis*. Chapman and Hall/CRC.

Hazen, E.L., Friedlaender, A.S., Thompson, M.A., Ware, C.R., Weinrich, M.T., Halpin, P.N. & Wiley, D.N. (2009) Fine-scale prey aggregations and foraging ecology of humpback whales *Megaptera novaeangliae*. *Marine Ecology Progress Series*, **395**, 75–89.

International Association of Geomagnetism and Aeronomy, Working Group V-MOD (2010) International geomagnetic reference field: the eleventh generation. *Geophysical Journal International*, **183**, 1216–1230.

Johnson, M., Aguilar de Soto, N. & Madsen, P.T. (2009) Studying the behaviour and sensory ecology of marine mammals using acoustic recording tags: a review. *Marine Ecology Progress Series*, **395**, 55–73.

Johnson, M.P. & Tyack, P.L. (2003) A digital acoustic recording tag for measuring the response of wild marine mammals to sound. *IEEE Journal of Oceanic Engineering*, **28**, 3–12.

Jonsen, I.D., Flemming, J.M. & Myers, R.A. (2005) Robust state-space modeling of animal movement data. *Ecology*, **86**, 2874–2880.

Jonsen, I., Basson, M., Bestley, S., Bravington, M., Patterson, T., Pedersen, M., Thomson, R., Thygesen, U. & Wotherspoon, S. (2012) State-space models for bio-loggers: A methodological road map. *Deep Sea Research Part II: Topical Studies in Oceanography*, **88–89**, 34–46.

643 Langrock, R., Marques, T.A., Thomas, L. & Baird, R.W. (2013) Modeling
644 the diving behavior of whales: a latent-variable approach with feedback
645 and semi-Markovian components. *Journal of Agricultural, Biological, and*
646 *Environmental Statistics*, **19**, 82–100.

647 Langrock, R., Hopcraft, J.G.C., Blackwell, P.G., Goodall, V., King, R., Niu,
648 M., Patterson, T.A., Pedersen, M.W., Skarin, A. & Schick, R.S. (2014)
649 A model for group dynamic animal movement. *Methods in Ecology &*
650 *Evolution*, **5**, 190–199.

651 Laplanche, C., Marques, T. & Thomas, L. (2015) Data from: Tracking ma-
652 rine mammals in 3D using electronic tag data. *Dryad Digital Repository.*
653 DOI:10.5061/dryad.138cg.

654 Laplanche, C. (2012) Bayesian three-dimensional reconstruction of toothed
655 whale trajectories: Passive acoustics assisted with visual and tagging mea-
656 surements. *The Journal of the Acoustical Society of America*, **132**, 3225–
657 3233.

658 Madsen, P.T., Johnson, M., de Soto, N.A., Zimmer, W.M.X. & Tyack, P.
659 (2005) Biosonar performance of foraging beaked whales (*Mesoplodon den-*
660 *sirostris*). *The Journal of Experimental Biology*, **208**, 181–194.

661 Marshall, G., Bakhtiari, M., Shepard, M., Tweedy III, J., Rasch, D., Aber-
662 nathy, K., Joliff, B., Carrier, J.C. & Heithaus, M.R. (2007) An ad-
663 vanced solid-state animal-borne video and environmental data-logging de-
664 vice ("Crittercam") for marine research. *Marine Technology Society Jour-*
665 *nal*, **41**, 31–38.

666 McClintock, B.T., King, R., Thomas, L., Matthiopoulos, J., McConnell, B.J.
667 & Morales, J.M. (2012) A general modeling framework for animal move-
668 ment and migration using multi-state random walks. *Ecological Mono-*
669 *graphs*, **82**, 335–349.

670 McClintock, B., London, J., Cameron, M. & Boveng, P. (2015) Modelling
671 animal movement using the argos satellite telemetry location error ellipse.
672 *Methods in Ecology and Evolution.*

673 Mitani, Y., Sato, K., Ito, S., Cameron, M.F., Siniff, D.B. & Naito, Y. (2003)
674 A method for reconstructing three-dimensional dive profiles of marine

675 mammals using geomagnetic intensity data: results from two lactating
676 weddell seals. *Polar Biology*, **26**, 311–317.

677 Morales, J.M., Haydon, D.T., Frair, J., Holsinger, K.E. & Fryxell, J.M.
678 (2004) Extracting more out of relocation data: building movement models
679 as mixtures of random walks. *Ecology*, **85**, 2436–2445.

680 Ntzoufras, I. (2009) *Bayesian modeling using WinBUGS*. Wiley series in
681 computational statistics. John Wiley & Sons, Inc., Hoboken, New Jersey.

682 O'Hara, R. & Sillanpää, M. (2009) A review of Bayesian variable selection
683 methods: What, how and which. *Bayesian Analysis*, **4**, 85–118.

684 R Core Team (2013) *R: A Language and Environment for Statistical Com-*
685 *puting*. R Foundation for Statistical Computing, Vienna, Austria.

686 Ropert-Coudert, Y. & Wilson, R.P. (2005) Trends and perspectives in
687 animal-attached remote sensing. *Frontiers in Ecology and the Environ-*
688 *ment*, **3**, 437–444.

689 Rutz, C. & Troscianko, J. (2013) Programmable, miniature video-loggers
690 for deployment on wild birds and other wildlife. *Methods in Ecology and*
691 *Evolution*, **4**, 114–122.

692 Shaffer, J.W., Moretti, D., Jarvis, S., Tyack, P. & Johnson, M. (2013) Ef-
693 fective beam pattern of the Blainville's beaked whale (*Mesoplodon den-*
694 *sirostris*) and implications for passive acoustic monitoring. *The Journal of*
695 *the Acoustical Society of America*, **133**, 1770–1784.

696 Shiomi, K., Sato, K., Mitamura, H., Arai, N., Naito, Y. & Ponganis, P.J.
697 (2008) Effect of ocean current on the dead-reckoning estimation of 3-D
698 dive paths of emperor penguins. *Aquatic Biology*, **3**, 265–270.

699 Simon, M., Johnson, M., Tyack, P. & Madsen, P.T. (2009) Behaviour and
700 kinematics of continuous ram filtration in bowhead whales (*Balaena mys-*
701 *ticetus*). *Proceedings of the Royal Society B: Biological Sciences*, **276**,
702 3819–828.

703 Simon, M., Johnson, M. & Madsen, P.T. (2012) Keeping momentum with
704 a mouthful of water: behavior and kinematics of humpback whale lunge
705 feeding. *The Journal of Experimental Biology*, **215**, 3786–3798.

706 Spiegelhalter, D., Best, N., Carlin, B. & van der Linde, A. (2002) Bayesian
707 measures of model complexity and fit. *Journal of the Royal Statistical*
708 *Society Series B*, **64**, 583–639.

709 Spiegelhalter, D., Best, N., Carlin, B. & van der Linde, A. (2014) The de-
710 viance information criterion: 12 years on. *Journal of the Royal Statistical*
711 *Society Series B*, **76**, 485–493.

712 Tracey, J.A., Sheppard, J., Zhu, J., Wei, F., Swaisgood, R.R. & Fisher, R.N.
713 (2014) Movement-based estimation and visualization of space use in 3D
714 for wildlife ecology and conservation. *PLoS ONE*, **9**, e101205.

715 Tyson, R.B., Friedlaender, A.S., Ware, C., Stimpert, A.K. & Nowacek,
716 D.P. (2012) Synchronous mother and calf foraging behaviour in hump-
717 back whales *Megaptera novaeangliae*: insights from multi-sensor suction
718 cup tags. *Marine Ecology Progress Series*, **457**, 209–220.

719 Ward, J., Jarvis, S., Moretti, D., Morrissey, R., DiMarzio, N., Thomas,
720 L. & Marques, T.A. (2011) Beaked whale (*Mesoplodon densirostris*) pas-
721 sive acoustic detection with increasing ambient noise. *The Journal of the*
722 *Acoustical Society of America*, **129**, 662–669.

723 Ware, C., Arsenault, R., Plumlee, M. & Wiley, D. (2006) Visualizing the
724 underwater behavior of humpback whales. *IEEE Computer Graphics and*
725 *Applications*, pp. 14–18.

726 Ware, C., Friedlaender, A.S. & Nowacek, D.P. (2011) Shallow and deep lunge
727 feeding of humpback whales in fjords of the West Antarctic Peninsula.
728 *Marine Mammal Science*, **27**, 587–605.

729 Ware, C., Wiley, D.N., Friedlaender, A.S., Weinrich, M., Hazen, E.L., Boc-
730 concelli, A., Parks, S.E., Stimpert, A.K., Thompson, M.A. & Abernathy,
731 K. (2014) Bottom side-roll feeding by humpback whales (*Megaptera no-*
732 *vaeangliae*) in the southern Gulf of Maine, U.S.A. *Marine Mammal Sci-*
733 *ence*, **30**, 494–511.

734 Watwood, S.L., Miller, P.J.O., Johnson, M., Madsen, P.T. & Tyack, P.L.
735 (2006) Deep-diving foraging behaviour of sperm whales (*Physeter macro-*
736 *cephalus*). *Journal of Animal Ecology*, **75**, 814–825.

737 Wilson, R.P., Liebsch, N., Davies, I.M., Quintana, F., Weimerskirch, H.,
738 Storch, S., Lucke, K., Siebert, U., Zankl, S., Muller, G., Zimmer, I., Sco-
739 laro, A., Campagna, C., Plotz, J., Bornemann, H., Teilmann, J. & McMa-
740 hon, C.R. (2007) All at sea with animal tracks; methodological and ana-
741 lytical solutions for the resolution of movement. *Deep Sea Research Part*
742 *II: Topical Studies in Oceanography*, **54**, 193 – 210.

743 Zimmer, W.M.X., Tyack, P.L., Johnson, M.P. & Madsen, P.T. (2005) Three-
744 dimensional beam pattern of regular sperm whale clicks confirms bent-horn
745 hypothesis. *The Journal of the Acoustical Society of America*, **117**, 1473–
746 1485.

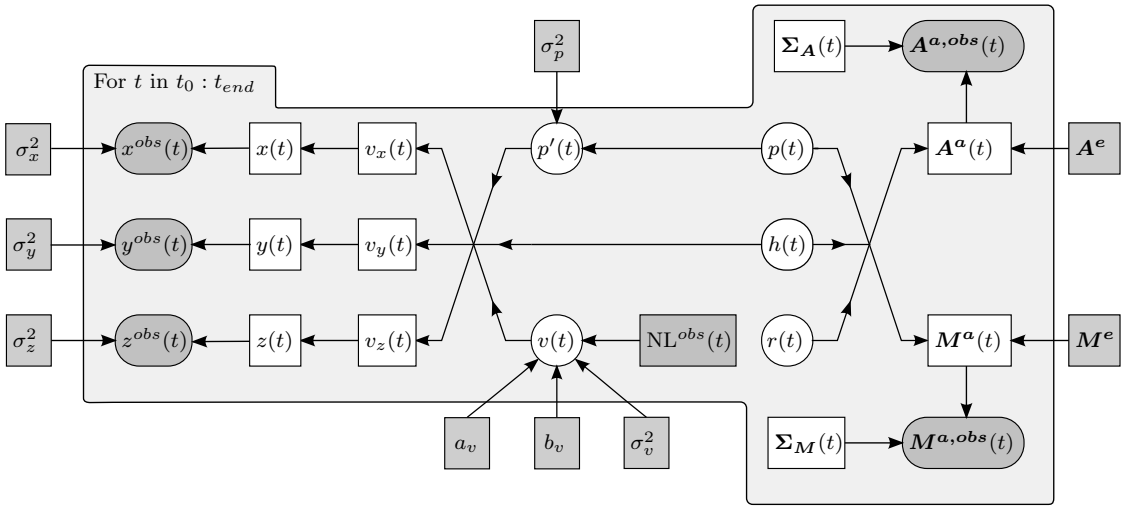

Figure 1: Directed acyclic graph (DAG) illustrating the relationship between model parameters and measured variables. Measured variables (in dark grey) are either modeled as random variables (circles and rounded rectangles) or are considered as known (rectangles). Parameters (in white) are either defined by a stochastic formula (circles and rounded rectangles) or are deterministic resultants of upstream nodes (rectangles). Variables indexed with t are time-dependent (grey polygon). The 3D orientation of the animal ($h(t)$, $p(t)$, $r(t)$) is estimated from the accelerometer and magnetometer ($\boldsymbol{A^{a,obs}}(t)$, $\boldsymbol{M^{a,obs}}(t)$) data. The 3D orientation and norm ($h(t)$, $p'(t)$, $v(t)$) of the animal speed vector is used to compute the 3D speed vector ($v_x(t)$, $v_y(t)$, $v_z(t)$) and resulting track ($x(t)$, $y(t)$, $z(t)$). The model allows for the possibility that the animal has a swimming direction ($p'(t)$) that is distinct from, yet statistically related to, the 3D orientation of its body ($p(t)$).

747

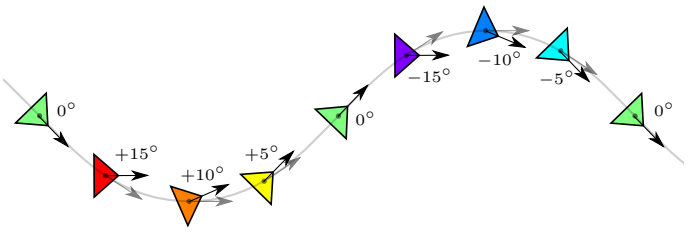

Figure 2: Pitch anomaly $\Delta p(t) = p(t) - p'(t)$ is the difference between the pitch ($p(t)$) of the orientation of the animal's longitudinal axis (black arrows) and the pitch ($p'(t)$) of the animal's speed vector (grey arrows). A positive pitch anomaly highlights movements when the animal points its longitudinal axis higher than expected by its swimming direction, and vice versa. The 3D whale track (grey line) and vectors are projected on a vertical plane. The color legend for pitch anomaly is the same as what is used in Figure 4 (green: no anomaly; from yellow to red: increasing positive anomaly; from cyan to violet: decreasing negative anomaly), angles between pairs of arrows have been inflated in the current plot for the ease of representation.

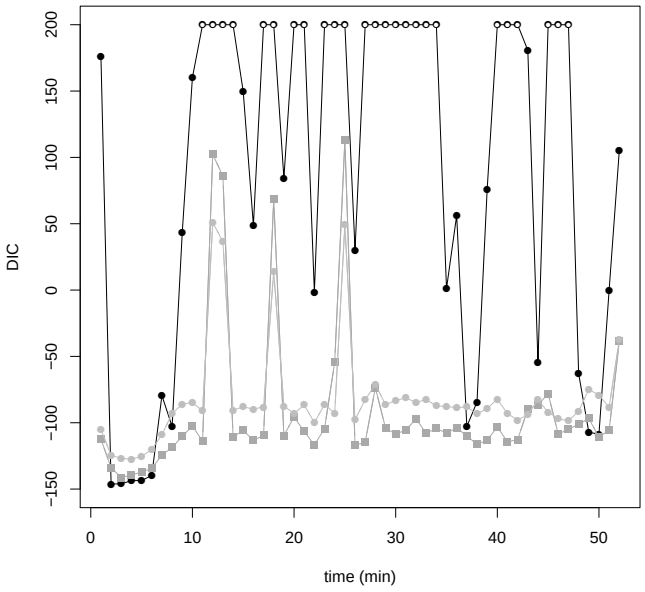

Figure 3: DIC values computed separately for each minute of the dive for models $\mathcal{M}_0$ (black dots, values greater than 200 are represented as empty dots), $\mathcal{M}_5$ (dark grey squares), and $\mathcal{M}_{10}$ (light grey circles).

748

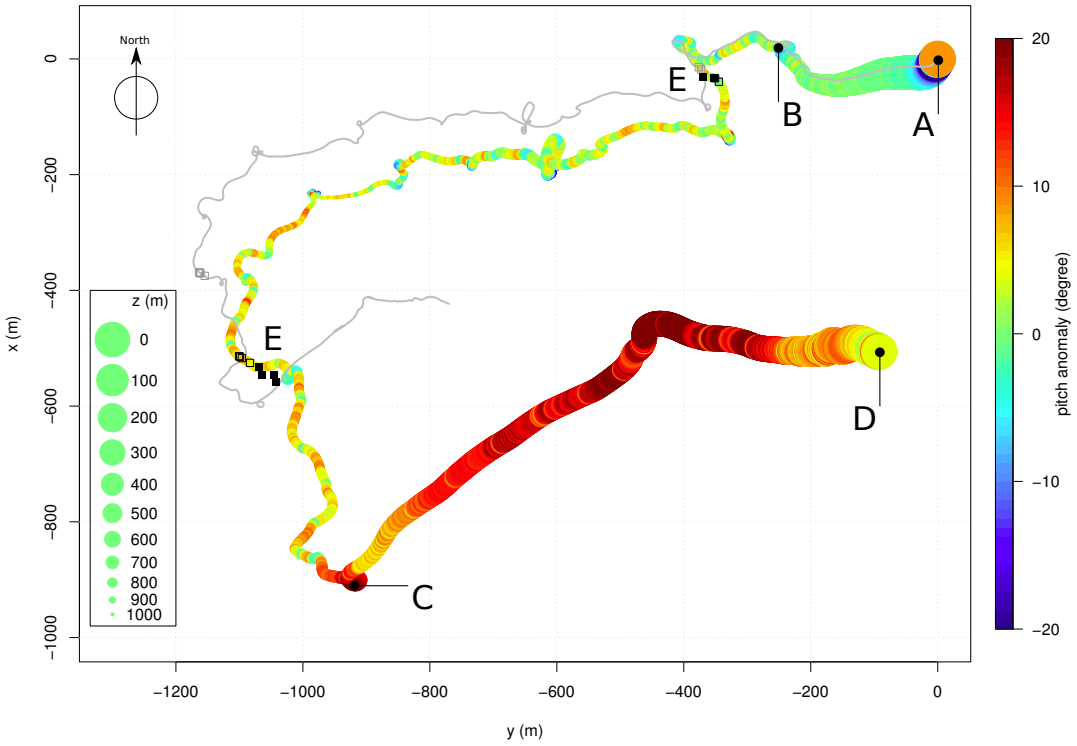

Figure 4: Estimated 3D whale track (x-axis, y-axis, dot size) and pitch anomaly (color). The whale dives at $t_0 = 0$ (A), ends its descent and starts to actively search for prey at depth at $t_B = 7'50$ (B), starts to reascend at $t_C = 35'30$ (C), and resurfaces at $t_{end} = 51'20$ (D). Independent acoustic localization from surrounding AUTEC hydrophones are represented (full black squares, E) together with points on the estimated track at the same timing (empty black squares). The whale covers a total curvilinear distance of 5170 m (descent (AB): 895 m; at depth (BC): 2845 m; ascent (CD): 1430 m). Estimated whale track by processing accelerometer, magnetometer, and depthmeter data with a Kalman filter is represented (grey line) together with location at acoustic localization timing (grey squares).

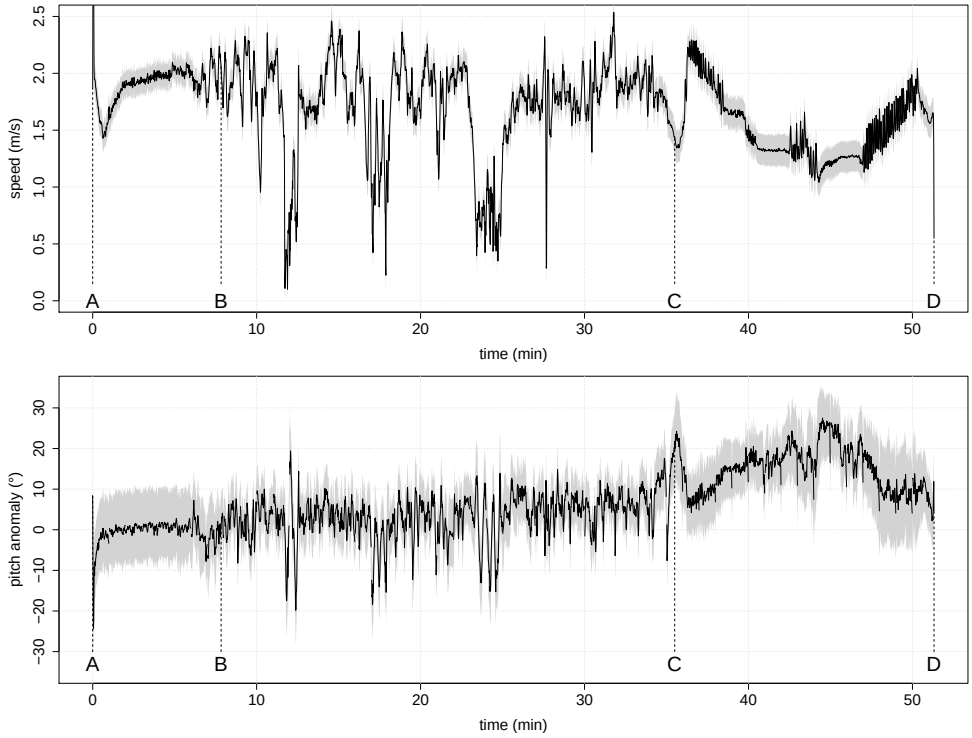

Figure 5: Point estimate of whale speed (top, in black) and pitch anomaly (bottom, in black). Descent (AB), at depth (BC), and ascent (CD) phases are defined in Figure 4. Mean speed during the descent is 1.91 ± 0.17 m/s, 1.72 ± 0.42 m/s at depth, and 1.51 ± 0.28 m/s during the ascent. Mean pitch anomaly is $-0.5 \pm 2.9°$ during the descent, $3.5 \pm 5.6°$ at depth, and $14.8 \pm 5.5°$ during the ascent. Interval estimates are also represented on the plots (in grey). At depth, sections of large speed are associated with small pitch anomaly variations, and vice versa.

Appendix S1 – Statistical model for accelerometer and magnetometer measurement errors

Accelerometer and magnetometer measurements normalized with respect to the norms of the earth gravitational and magnetic fields, $\boldsymbol{A}^{\boldsymbol{a,obs}}(t)/||\boldsymbol{A}^{\boldsymbol{e}}||$ and $\boldsymbol{M}^{\boldsymbol{a,obs}}(t)/||\boldsymbol{M}^{\boldsymbol{e}}||$, would have a constant unit norm if earth gravitational and magnetic fields were the only components in accelerometer and magnetometer measurements. In practice, both norms are time-dependent, as a result of other sources of acceleration, plus noise. By modelling errors on each of the 3 accelerometer coordinates as independent and normally distributed (discussed below) with variances $\sigma_A^2(t)$, the variance of the squared norm $[||\boldsymbol{A}^{\boldsymbol{a,obs}}(t)||/||\boldsymbol{A}^{\boldsymbol{e}}||]^2$ is $6\sigma_A^4(t) + 4\sigma_A^2(t) \simeq 4\sigma_A^2(t)$ (by neglecting the fourth-order term, since $\sigma_A \ll 1$; see values below for $\sigma_A(t)$). One can find a similar formula for the variance of the squared norm $[||\boldsymbol{M}^{\boldsymbol{a,obs}}(t)||/||\boldsymbol{M}^{\boldsymbol{e}}||]^2$. Consequently, the time-dependent covariance matrices in equation (3) are here diagonals, $\boldsymbol{\Sigma_A}(t) = \sigma_A^2(t)I$ and $\boldsymbol{\Sigma_M}(t) = \sigma_M^2(t)I$, with variances $\sigma_A^2(t)$ and $\sigma_M^2(t)$ equal to a quarter of the variances of the norms $||\boldsymbol{A}^{\boldsymbol{a,obs}}(t)||/||\boldsymbol{A}^{\boldsymbol{e}}||$ and $||\boldsymbol{M}^{\boldsymbol{a,obs}}(t)||/||\boldsymbol{M}^{\boldsymbol{e}}||$ which are directly measurable. Plots of $||\boldsymbol{A}^{\boldsymbol{a,obs}}(t)||$ and $||\boldsymbol{M}^{\boldsymbol{a,obs}}(t)||$ (not shown) strongly suggest consideration of distinct but constant variances for the animal descent, active searching for prey, and ascent (sequences AB, BC, and CD illustrated in Figure 4). Computed values are respectively for these three stages 1.12, 1.90, and 1.12 % for $\sigma_A(t)$ and 0.61, 0.97, and 0.33 % for $\sigma_M(t)$.

Low resulting errors on orientation estimates (standard deviations on orientation angles are 0.78° on average, cf. main document's results section) and location estimates could be potentially biased, as discussed in the main document. Errors in orientation and location estimates are computed assuming the model is true. Possible improvements to the error structure might include (i) considering correlated errors across the three magnetometer and accelerometer axes, leading to non diagonal covariance matrices $\boldsymbol{\Sigma_A}(t)$ and $\boldsymbol{\Sigma_M}(t)$, (ii) considering auto-correlated errors, and (iii) using non-Gaussian distributions, particularly distributions defined on the circle.

Appendix S2 – Statistical model for speed from background noise level

Animal speed can theoretically be estimated ($v^{est}(t)$) from accelerometer, magnetometer, and depthmeter data alone

$$v^{est}(t) = |v_z(t)|\sqrt{1 + 1/\tan p(t)} \tag{S2–1}$$

where $v_z(t) = (z(t + \Delta t) - z(t))/\Delta t$ is the vertical speed computed from depth meter data and $p(t)$ is the pitch of the animal computed from the accelerometer and magnetometer. The use of equation (S2–1) is problematic for two main reasons. The first is that accelerometer, magnetometer, and depthmeter data provide no information on animal speed when the animal is horizontal (equation (S2–1) does not apply if $p(t) = 0$). As a corollary, the computation of animal speed from accelerometer, magnetometer, and depthmeter data with low pitch values is unreliable and highly sensitive to measurement error. The second reason is that, as considered in the present paper, animal orientation is not necessarily the orientation of its speed vector $\boldsymbol{v}(t)$, and consequently speed computed from accelerometer, magnetometer, and depthmeter data could be misleading. One could, however, use Equation (S2–1) to compute a reliable estimate of the speed norm from accelerometer, magnetometer, and depthmeter for periods of high pitch when the equal pitch assumption is likely to hold. As Simon et al. (2009), we consider the section of the dive when the animal is fluking and steeply descends from the sea surface to reach the foraging depth, and hence when the equal pitch assumption is most likely to hold. We apply equation (S2–1) to all samples ($n = 384$) during the animal descent for which the pitch is greater than 60° (an arbitrary threshold).

Background acoustic noise level is expected to increase with animal speed as a consequence of water flow on the sensor. Figure S2.1 shows the observed relationship between estimated speed for the above data versus measured noise level on the tag (on a logarithmic scale). An ordinary linear regression yielded the relationship, for data from descent with pitch > 60° of $E\{v(t)\} = 4.53 + 1.16 \log_{10}(\mathrm{NL}(t))$, with a residual standard error $\sigma_v = 0.08$ m/s ($R^2 = 0.77$). The fit is shown in Figure S2.1.

Also shown in Figure S2.1 are the samples ($n = 330$) during the animal ascent for which the pitch is greater than 60°. A similar regression on these data yielded somewhat different regression parameters ($E\{v(t)\} = 4.73 + 1.37 \log_{10}(\mathrm{NL}(t))$, with a residual standard error $\sigma_v = 0.12$ m/s, $R^2 = 0.84$). We postulate that ascent should not be considered to calibrate the speed-noise relationship, as during this stage the direction of the movement differs

from the animal's axis (Figure S2.2: on two occasions a positive pitch, i.e. head oriented upwards, is observed concurrently with a negative vertical speed, i.e. animal moving downwards). We hypothesize that the discrepancy between the descent and ascent calibration results (Figure S2-1) is that for the latter movement direction can differ from the animal's longitudinal axis. We therefore calibrated the speed-noise relationship with descent data, when the animal is actively navigating downwards, to predict animal speed from the noise level for the rest of the dive.

Currently this model does not consider differences of flow noise due to animal orientation and does not propagate errors on estimates a_v, b_v, and σ_v to location uncertainties. This is discussed in the main document.

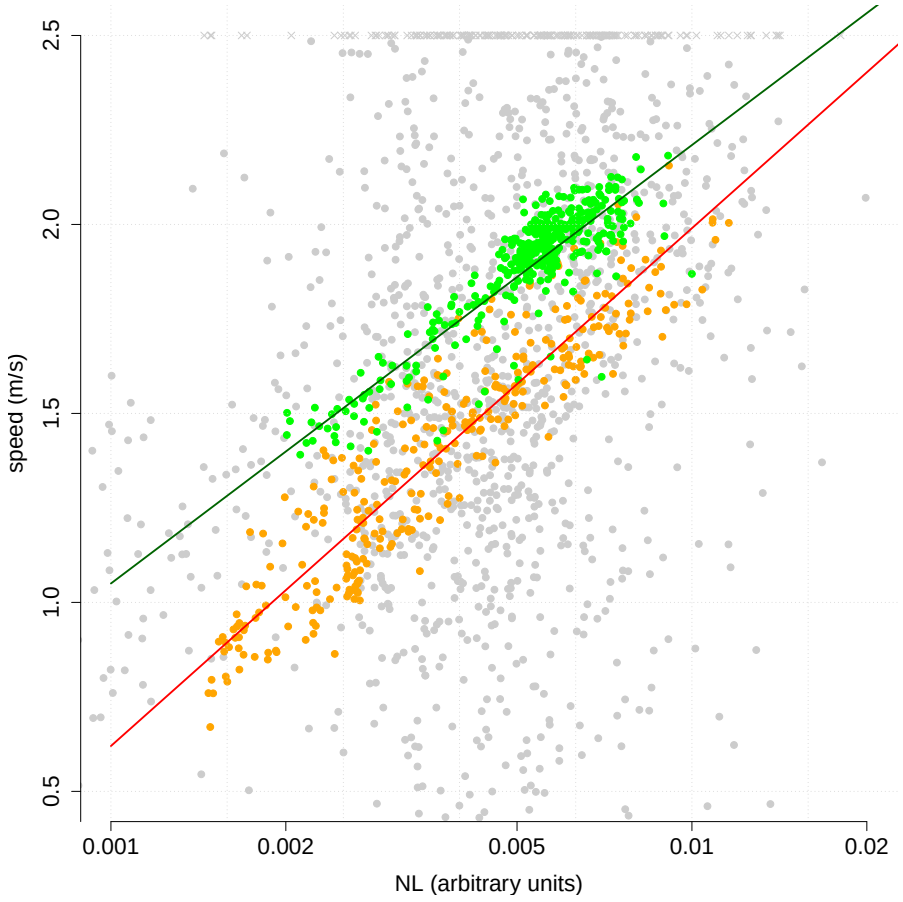

Figure S2.1: Measured noise level (NL) and speed norm (v) computed by dead reckoning from accelerometer, magnetometer, and depthmeter data. Samples with pitch angle $p(t) \geq 60°$ during the whale descent ($t \in [0, 470]$ s; 384 samples; in green), during the ascent ($t \in [2130, 3080]$ s; 330 samples; in orange), and remaining points (in grey; for a better presentation of points during the descent and the ascent, speed values greater than 2.5 m/s are censored and are represented as crosses). Speed is linearly related to the logarithm of the noise level by using data from the descent ($R^2 = 0.77$; green line) or the ascent ($R^2 = 0.84$; red line). Data from the descent are used to calibrate the relationship connecting v to NL. Predicted speed norm is $\mathrm{E}(v) = a_v + b_v \log_{10}(\mathrm{NL})$ ($a_v = 4.53$, $b_v = 1.16$), standard error is $\sigma_v = 0.08$ m/s.

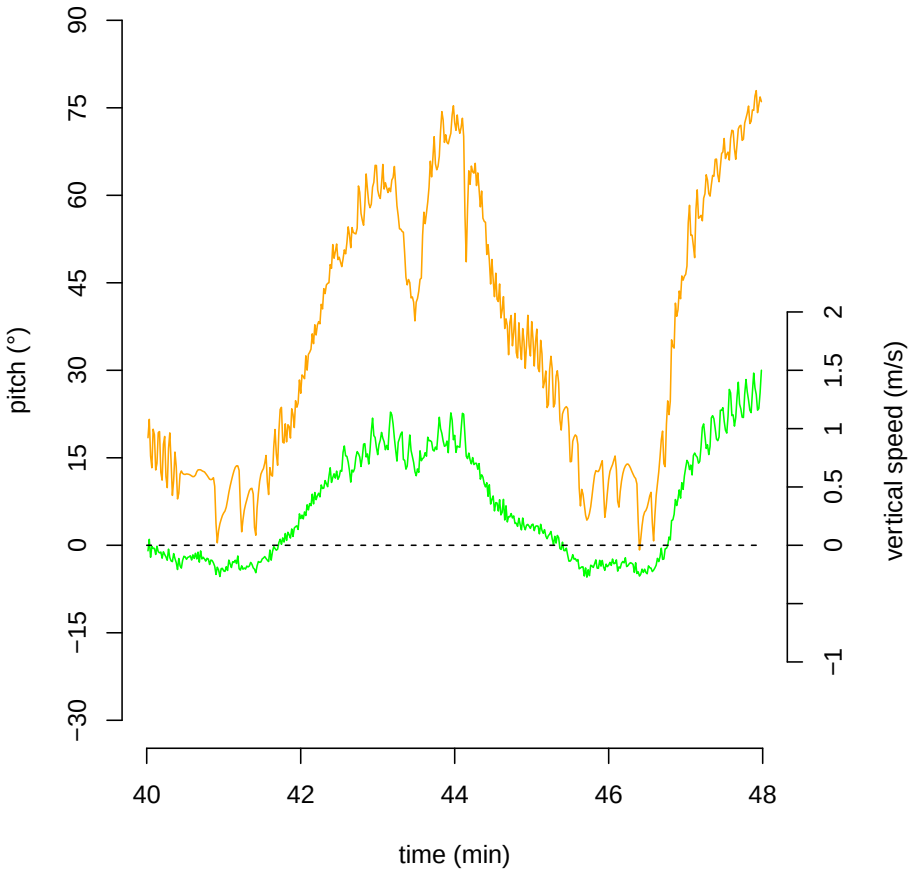

Figure S2.2: Pitch and vertical speed during the whale ascent. Pitch is computed from the accelerometer and accelerometer data (orange) and vertical speed is computed from the depth sensor data (green). On two occasions (around $t = 41$ and $t = 46$ minutes), the animal is oriented upwards (pitch is positive) while moving downwards (vertical speed is negative), showing that the direction of the animal movement is different from its longitudinal axis. Therefore, the equal pitch assumption does not to hold during the ascent, and the calibration of the relationship from the noise level during this stage is ill-advised.

Appendix S3 – BUGS code

As detailed in Appendix S4, computations are completed in three steps (CS 1, CS 2, CS 3). First, animal 3D orientation is computed from accelerometer and magnetometer data by simulating BUGS model `orientation` (code below). Second, parameters of the relationship connecting speed to noise level are found by regression (Appendix S2). Third, animal 3D track is computed from the animal orientation found in CS 1, regression parameters found in CS 2, and depth and noise level data, by simulating BUGS model `track` (code below). Propagation of errors from measurements to 3D track is described in Appendix S4.

Index $i \in \{1, \ldots, I\}$ is an index over time stamps, I is the number of time stamps, and time for index i is denoted `t_i[i]`. Although the track considered in this study was processed at a constant, 1-second time step, the BUGS code has been written to deal with any time step (smaller, larger, or adaptive). Time stamps are provided as data to the BUGS models.

In the orientation BUGS model, `sigma_A` and `sigma_M` refer to the standard deviations of the norms of $||\boldsymbol{A}^{\boldsymbol{a,obs}}(t)||/||\boldsymbol{A}^{\boldsymbol{e}}||$ and $||\boldsymbol{M}^{\boldsymbol{a,obs}}(t)||/||\boldsymbol{M}^{\boldsymbol{e}}||$ (see Appendix S1). Such values are behavioral state-dependent and are therefore indexed by `I_state` (descent: 1, searching for prey: 2, ascent: 3). Variables `sigma_A_i[i]` and `sigma_M_i[i]` refer to $\sigma_A(t)$ and $\sigma_M(t)$, which are equal to half `sigma_A` and `sigma_M` (Appendix S1). Since `sigma_A_i[i]` and `sigma_M_i[i]` represent the standard deviation of the average accelerometer and magnetometer error over a time step of duration `t_i[i+1]-t_i[i]` – while `sigma_A` and `sigma_M` are values for a 1-second time step – values `sigma_A_i[i]` and `sigma_M_i[i]` need to be adjusted in case of time steps smaller or larger than 1 second, which is achieved, by still assuming independent accelerometer and magnetometer errors, by dividing by `sqrt(t_i[i+1]-t_i[i])`.

```
model orientation {
  # heading , pitch, roll of the whale
  # earth frame
  for(i in 1:I){
    # heading
    h_i[i] ~ dunif(-180,180)
    h_cos_i[i] <- cos(h_i[i]/180*pi)
    h_sin_i[i] <- sin(h_i[i]/180*pi)
    # pitch
    p_i[i] ~ dunif(-90,90) # used by the acc/mag data model
    p_cos_i[i] <- cos(p_i[i]/180*pi)
```

```
  p_sin_i[i] <- sin(p_i[i]/180*pi)
  # roll
  r_i[i] ~ dunif(-180,180)
  r_cos_i[i] <- cos(r_i[i]/180*pi)
  r_sin_i[i] <- sin(r_i[i]/180*pi)
}
# acceleration and magnetic field
# earth frame
for(i in 1:I){
  Ax_earth_i[i] <- 0#ax_i[i]
  Ay_earth_i[i] <- 0#ay_i[i]
  Az_earth_i[i] <- -g#+az_i[i]
  Mx_earth_i[i] <- bx
  My_earth_i[i] <- by
  Mz_earth_i[i] <- bz
}
# acceleration and magnetic field
# whale frame
for(i in 1:I){
  Ax_whale_i[i] <- p_cos_i[i]*h_cos_i[i]*Ax_earth_i[i]+p_cos_i[i
     ]*h_sin_i[i]*Ay_earth_i[i]+p_sin_i[i]*Az_earth_i[i]
  Ay_whale_i[i] <- (-r_cos_i[i]*h_sin_i[i]-r_sin_i[i]*p_sin_i[i
     ]*h_cos_i[i])*Ax_earth_i[i]+(r_cos_i[i]*h_cos_i[i]-r_sin_i[
     i]*p_sin_i[i]*h_sin_i[i])*Ay_earth_i[i]+p_cos_i[i]*r_sin_i[
     i]*Az_earth_i[i]
  Az_whale_i[i] <- (r_sin_i[i]*h_sin_i[i]-r_cos_i[i]*p_sin_i[i]*
     h_cos_i[i])*Ax_earth_i[i]+(-r_sin_i[i]*h_cos_i[i]-r_cos_i[i
     ]*p_sin_i[i]*h_sin_i[i])*Ay_earth_i[i]+r_cos_i[i]*p_cos_i[i
     ]*Az_earth_i[i]
  Ax_whale_mes_i[i] ~ dnorm(Ax_whale_i[i],pi_A_i[i])
  Ay_whale_mes_i[i] ~ dnorm(Ay_whale_i[i],pi_A_i[i])
  Az_whale_mes_i[i] ~ dnorm(Az_whale_i[i],pi_A_i[i])
  Mx_whale_i[i] <- p_cos_i[i]*h_cos_i[i]*Mx_earth_i[i]+p_cos_i[i
     ]*h_sin_i[i]*My_earth_i[i]+p_sin_i[i]*Mz_earth_i[i]
  My_whale_i[i] <- (-r_cos_i[i]*h_sin_i[i]-r_sin_i[i]*p_sin_i[i
     ]*h_cos_i[i])*Mx_earth_i[i]+(r_cos_i[i]*h_cos_i[i]-r_sin_i[
     i]*p_sin_i[i]*h_sin_i[i])*My_earth_i[i]+(p_cos_i[i]*r_sin_i
     [i])*Mz_earth_i[i]
  Mz_whale_i[i] <- (r_sin_i[i]*h_sin_i[i]-r_cos_i[i]*p_sin_i[i]*
     h_cos_i[i])*Mx_earth_i[i]+(-r_sin_i[i]*h_cos_i[i]-r_cos_i[i
     ]*p_sin_i[i]*h_sin_i[i])*My_earth_i[i]+(r_cos_i[i]*p_cos_i[
     i])*Mz_earth_i[i]
  Mx_whale_mes_i[i] ~ dnorm(Mx_whale_i[i],pi_M_i[i])
  My_whale_mes_i[i] ~ dnorm(My_whale_i[i],pi_M_i[i])
  Mz_whale_mes_i[i] ~ dnorm(Mz_whale_i[i],pi_M_i[i])
```

```
  }
  # standard deviations and precisions
  # accelerometer and magnetometer data
  for(i in 1:I){
    # the sd of one 3d coordinate component is half the sd of the
       norm
    # A and M are averages over t_i[i+1]-t_i[i] samples
    sigma_A_i[i] <- sigma_A[I_state[i]]/sqrt(t_i[i+1]-t_i[i])/2
    sigma_M_i[i] <- sigma_M[I_state[i]]/sqrt(t_i[i+1]-t_i[i])/2
    pi_A_i[i] <- 1/(sigma_A_i[i]*sigma_A_i[i])
    pi_M_i[i] <- 1/(sigma_M_i[i]*sigma_M_i[i])
  }
}
```

```
model track {
  # heading, pitch, roll of the whale
  # EARTH frame
  for(i in 1:I){
    # heading
    h_i[i] ~ dnorm(h_mes_i[i],pi_h_i[i])I(-180,180) # from the acc
       /mag data model
    # pitch
    p_i[i] ~ dnorm(p_mes_i[i],pi_p_i[i])I(-90,90) # from the acc/
       mag data model
    pprime_i[i] ~ dnorm(p_i[i],pi_p)I(-90,90)
    dp_i[i] <- p_i[i]-pprime_i[i]
  }
  # speed (m/s)
  # EARTH frame
  for(i in 1:I){
    v_pred_i[i] <- a_v+b_v*log(noiselevel[i])/log(10)
    v_i[i] ~ dnorm(v_pred_i[i],pi_v)I(0,)
  }
  for(i in 1:I){
    vx_i[i] <- cos(h_i[i]/180*pi)*cos(pprime_i[i]/180*pi)*v_i[i]
    vy_i[i] <- -sin(h_i[i]/180*pi)*cos(pprime_i[i]/180*pi)*v_i[i]
    vz_i[i] <- sin(pprime_i[i]/180*pi)*v_i[i]
  }
  # location (m)
  # EARTH frame
  x_i[1] <- 0
  y_i[1] <- 0
  z_i[1] ~ dnorm(0,1.0E-8)I(,0)
  for(i in 1:I){
    x_i[i+1] <- x_i[i]+vx_i[i]*(t_i[i+1]-t_i[i])
```

```
    y_i[i+1] <- y_i[i]+vy_i[i]*(t_i[i+1]-t_i[i])
    z_i[i+1] <- z_i[i]+vz_i[i]*(t_i[i+1]-t_i[i])
  }
  # whale known location
  for(i_mes_xy in 1:I_mes_xy){
    x_mes_i[i_mes_xy] ~ dnorm(x_i[i_mes_xy_i[i_mes_xy]],pi_x_i[
        i_mes_xy])
    y_mes_i[i_mes_xy] ~ dnorm(y_i[i_mes_xy_i[i_mes_xy]],pi_y_i[
        i_mes_xy])
  }
  # whale depth (from depth-meter)
  for(i in 1:(I+1)){
    z_mes_i[i] ~ dnorm(z_i[i],pi_z_i[i])I(,0)
  }
  # standard deviations and precisions
  # known location
  for(i_mes_xy in 1:I_mes_xy){
    pi_x_i[i_mes_xy_i[i_mes_xy]] <- 1/(sigma_x_i[i_mes_xy_i[
        i_mes_xy]]*sigma_x_i[i_mes_xy_i[i_mes_xy]])
    pi_y_i[i_mes_xy_i[i_mes_xy]] <- 1/(sigma_y_i[i_mes_xy_i[
        i_mes_xy]]*sigma_y_i[i_mes_xy_i[i_mes_xy]])
  }
  # depth
  for(i in 1:(I+1)){
    sigma_z_i[i] <- sigma_z
    pi_z_i[i] <- 1/(sigma_z_i[i]*sigma_z_i[i])
  }
  # speed
  pi_v <- 1/(sigma_v*sigma_v)
  # angles
  pi_p <- 1/(sigma_p*sigma_p)
  for(i in 1:I){
    pi_p_i[i] <- 1/(sigma_p_i[i]*sigma_p_i[i])
    pi_h_i[i] <- 1/(sigma_h_i[i]*sigma_h_i[i])
  }
}
```

Appendix S4 – Procedure to distribute track computations on a High Performance Resource (HPR)

The HBM presented in the main document could theoretically be used to process tag data and compute animal 3D orientation and location for the complete track. Computation time for this is, however, prohibitive given the large number of parameters (3D orientation, speed and location at each time step) to be simulated by the MCMC sampler. In order to speed up computations, the parameter estimation procedure is completed in three consecutive steps. First (later referred to as Computation Step 1, CS 1), point estimates of the heading, pitch, and roll (denoted $h^{est}(t)$, $p^{est}(t)$, and $r^{est}(t)$) and respective variances ($\sigma_h^2(t)$, $\sigma_p^2(t)$, and $\sigma_r^2(t)$) are computed from the accelerometer and magnetometer data by simulating the HBM defined by equations (1) to (4). The BUGS code for this reduced model is provided in Appendix S3. Second (CS 2), parameters of the relationship connecting speed to noise level are found by using noise level data, depth data, and point estimates of the animal pitch found in CS 1 (details are provided in Appendix S2). Third (CS 3), animal 3D track is computed from the orientation found in CS 1, regression parameters found in CS 2, depth data, and noise level data. In CS 3, the animal location and orientation are simulated by using the priors

$$\begin{cases} h(t) \sim \text{Normal}(h^{est}(t), \sigma_h^2(t)) \\ p(t) \sim \text{Normal}(p^{est}(t), \sigma_p^2(t)) \end{cases} \tag{S2–2}$$

together with the HBM defined by equations (5) to (10). The BUGS code for this reduced model is also provided in Appendix S3. Initializations for CS1 were computed by adding noise to accelerometer and magnetometer data (using noise model described in Appendix S1) before calculating heading, pitch, and roll as suggested by Johnson & Tyack (2003). Initializations for CS3 were computed by adding noise to heading and pitch output from CS1 (using equation S2–2) as well as to depth measured values and by reconstructing tracks by dead-reckoning.

To take advantage of high performance resources (HPR), animal location and orientation (CS 1 and 3) are computed by splitting the whole track into m consecutive pieces (time stamps are relabeled $t_{j,i} = t_0 + \sum_{j'=1}^{j-1} \Delta t_{j'} + i$, Δt_j is the duration of piece $j \in \{1, \ldots, m\}$, $i \in \{0, \ldots, \Delta t_j\}$). Tag data at time $t \in [t_0, t_{end}]$ provide information on the orientation of the animal only for time t and information on the location of the animal only for subsequent timing $[t, t_{end}]$. Consequently, computation of animal orientation (CS 1) for all pieces can be carried out independently of each other and computation

of animal location (CS 3) can be carried out sequentially. The error on the animal estimated location at the end of some piece $j \in \{1, \ldots, m-1\}$ is propagated as an error on the 'observed' location at the beginning of piece $j+1$. This could be achieved by updating equation (9) accordingly, the 'observed' coordinates of the animal at time $t_{j+1,0}$ would be in that case

$$\begin{cases} x(t_{j+1,0}) \sim \text{Normal}(x^{est}(t_{j,\Delta_j}), \sigma_x^2(t_{j,\Delta_j})) \\ y(t_{j+1,0}) \sim \text{Normal}(y^{est}(t_{j,\Delta_j}), \sigma_y^2(t_{j,\Delta_j})) \end{cases} \quad \text{(S2–3)}$$

where $x_j^{est}(t_{j,\Delta_j})$, $y_j^{est}(t_{j,\Delta_j})$ are the point estimated x- and y- coordinates of the animal at time t_{j,Δ_j} and $\sigma_x^2(t_{j,\Delta_j})$, $\sigma_y^2(t_{j,\Delta_j})$ their respective variances. Computations for pieces $j \in \{1, \ldots, m\}$ would still need to be carried out one after the other (simulation of piece j requires the output for piece $j-1$) and could not be parallelized in order to take benefit from HPR. Another option is to carry out CS 3 for all pieces independently of each other and to propagate localization errors by post-processing. In that case, CS 3 is performed by setting $x(t_{j,0})$ and $y(t_{j,0})$ to zero with null variances ($j \in \{1, \ldots, m\}$). For $j = 1$ to $j = m-1$, the point estimate and the variance of the location estimate at time t_{j,Δ_j} are added to the point estimates and variances of the location estimate for times $t_{j+1,0}$ to $t_{j+1,\Delta_{j+1}}$. This option, enabling the distribution of track computations on a HPR, has been applied in order to produce the results presented in the main document.

The complete track was split into 51 1-minute consecutive pieces and a remaining 20-second piece ($m = 52$, $\Delta t_j = 60$ for $j \in \{1, \ldots, 51\}$, $\Delta t_{52} = 20$). Computation of the orientation of the animal (CS 1) and of the location of the animal (CS 3) required the simulation of $11,000$ and $20,000$ samples per chain, respectively (see Section 2.3 for more details). For each 1-minute piece, and for each chain, CS 1 and CS 3 respectively required 20 s and 75 minutes of computation time on a single core of an Intel® Xeon E5-2680v2 2.8Ghz 10-core processor. The computation time for the complete dive is consequently of approximately 65 h, which is reduced to 75 minutes by using HPR on 52 cores. Simulation of 4 chains required 5 hours, which could have been reduced to 75 minutes by using 208 cores.

The HPR used in this study (EOS) is structured into 1224 Intel® Xeon E5-2680v2 2.8GHz 10-core processors which are scheduled and controlled by the SMURL resource manager. Simulations were dispatched to 6 processors (60 cores) by using CHDB software running with Intel® MPI library. CHDB (http://www.calmip.univ-toulouse.fr/spip/spip.php?article465) was originally designed for bioinformatics purposes to drive the processing of large number of data files on a cluster by the repeated use of a single program. In our case, we used CHDB to process BUGS batch files – one file

per track piece and initialization – with BUGS software. An example of a batch file (here first initialization of the first track piece) is provided below.

```
modelCheck('model/m6_track.R')
modelData('data/data_m6_tC1.txt')
modelCompile(1)
modelInits('init/init_m6_tC1_chain1.txt',1)
modelUpdate(1000,10)
modelSaveState('log/state_m6_tC1_chain1.txt')
samplesSet('deviance')
samplesSet('h_i')
samplesSet('p_i')
samplesSet('pprime_i')
samplesSet('dp_i')
samplesSet('x_i')
samplesSet('y_i')
samplesSet('z_i')
samplesSet('v_i')
modelUpdate(1000,10)
samplesStats('*')
modelSaveState('log/state_m6_tC1.txt')
#samplesCoda('*','coda/coda_m6_tC1_chain1.txt')
modelQuit()
```

BUGS output files (table containing parameter statistics) were later loaded into R and merged together (post-processing described earlier) by using R code below:

```
TRACK=read.table(paste('track/track_tC1.txt',sep=''),header=TRUE)
for(i_traj_id in 2:52){
  traj_id=paste('C',i_traj_id,sep='')
  TRACK_i=read.table(paste('track/track_t',traj_id,'.txt',sep=''),
     header=TRUE)
  # point and interval estimates for heading (h), pitch (p), roll
     (r), speed norm (v)
  # just copy-paste
  TRACK[c('h','p','p2','r','v','h_val2.5pc','h_val97.5pc','p_val2
     .5pc','p_val97.5pc','r_val2.5pc','r_val97.5pc','p2_val2.5pc
     ','p2_val97.5pc','v_val2.5pc','v_val97.5pc','dp_val2.5pc','
     dp_val97.5pc')][nrow(TRACK),]=TRACK_i[c('h','p','p2','r','v
     ','h_val2.5pc','h_val97.5pc','p_val2.5pc','p_val97.5pc','
     r_val2.5pc','r_val97.5pc','p2_val2.5pc','p2_val97.5pc','
```

```
    v_val2.5pc','v_val97.5pc','dp_val2.5pc','dp_val97.5pc')][1,]
  # point estimates for horizontal location (x and y)
  # add
  TRACK_i['x']=TRACK_i['x']+TRACK['x'][nrow(TRACK),]
  TRACK_i['y']=TRACK_i['y']+TRACK['y'][nrow(TRACK),]
  # variances for horizontal location (x and y)
  # add
  TRACK_i['x_sd']=sqrt(TRACK_i['x_sd']^2+TRACK['x_sd'][nrow(TRACK)
    ,]^2)
  TRACK_i['y_sd']=sqrt(TRACK_i['y_sd']^2+TRACK['y_sd'][nrow(TRACK)
    ,]^2)
  TRACK=rbind(TRACK,TRACK_i[-1,])
}
# interval estimates for horizontal location (x and y)
TRACK$x_val2.5pc=TRACK$x-2*TRACK$x_sd
TRACK$x_val97.5pc=TRACK$x+2*TRACK$x_sd
TRACK$y_val2.5pc=TRACK$y-2*TRACK$y_sd
TRACK$y_val97.5pc=TRACK$y+2*TRACK$y_sd
write.table(TRACK,'track_full.txt',quote=FALSE)
```

Appendix S6 – Investigating sensitivity to variance in pitch anomaly and flow noise relationship

Animal track in this study was reconstructed by using the speed-noise relationship calibrated using data from the animal descent ($a_v = 4.53$, $b_v = 1.16$, $\sigma_v = 0.08$) with a moderate pitch anomaly ($\sigma_p = 5°$). One could theoretically calibrate the speed-noise relationship using data from the animal ascent, although this appears strongly ill-advised since during this stage the direction of the movement differs from the animal's axis (Appendix S2). One could also consider a higher pitch anomaly ($\sigma_p = 10°$), although once again this seems ill-advised since model comparison strongly suggested to consider the more moderate value $\sigma_p = 5°$. Nevertheless, to explore the sensitivity of the localization process to such choices, we compare the animal track's reconstruction considering the 4 possible combinations of: (1) either the animal descent or ascent to calibrate the speed-noise relationship and (2) either moderate ($\sigma_p = 5°$) or high ($\sigma_p = 10°$) pitch anomaly (Figure S6-1). The distance between the track presented in the main document and (respectively) the track using data from the animal descent and $\sigma_p = 10°$, data from the animal ascent and $\sigma_p = 5°$, and data from the animal ascent and $\sigma_p = 10°$ are 17.4 ± 14.5 m, 124.6 ± 70.5 m, and 173.9 ± 92.6 m. As discussed, the model, while considering various sources of errors, assumes that parameters a_v, b_v, σ_v, and σ_p are perfectly known. We therefore highlight (i) the critical choice for 'known' parameters (in this case a_v, b_v, σ_v, and σ_p) in the track reconstruction process and the need, as was done here, to support the choice of their values from data, and (ii) the underestimate of confidence intervals width on estimated locations since variances of parameter estimates are conditional on the model being true, which ignores additional variability not accounted for in the model. In our case, results ignore errors originating from the divergence between the truth and the model for the speed-noise relationship (inaccurate parameter values or relationship) and the pitch anomaly process (inaccurate parameter value or relationship).

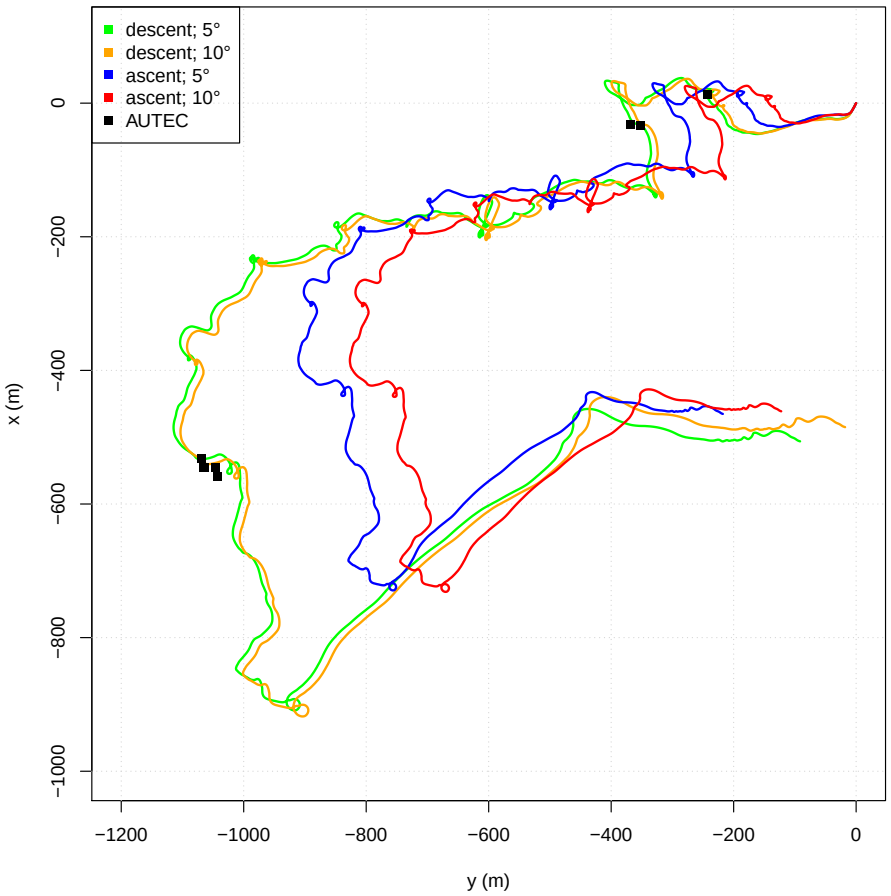

Figure S6.1: Reconstructed track for different options of calibration of the speed-noise relationship and different amplitude of pitch anomaly. The track presented in the main document (green; color line in Figure 4) has been reconstructed by calibrating the speed-noise relationship using data from the animal descent with a moderate pitch anomaly ($\sigma_p = 5°$). Other options are considered (orange: calibration using data from the descent, $\sigma_p = 10°$; blue: ascent, $\sigma_p = 5°$; red: ascent, $\sigma_p = 10°$). Locations found from the independent acoustic survey are also plotted (black dots).